Determination of the Three-Dimensional Structure of CC Chemokine Monocyte Chemoattractant Protein 3 by ^{1}H Two-Dimensional NMR Spectroscopy‡

S. Meunier,§,# J.-M. Bernassau,|| J.-C. Guillemot,⊥ P. Ferrara,⊥ and H. Darbon*,§

AFMB-IFR1, UPR 9039-CNRS, 31 chemin Joseph Aiguier, 13402 Marseille Cedex 20, France, SANOFI Recherche, 371 rue du Pr Joseph Blayac, 34184 Montpellier Cedex 04, France, and SANOFI-Elf Bio Recherche, Labege Innopole Voie No. 1, BP 137, 31876 Labege Cedex, France

Received November 11, 1996; Revised Manuscript Received January 24, 1997⊗

ABSTRACT: MCP-3 is a β chemokine consisting of 76 amino acid residues. It has been described to be involved in the activation of all leukocytic cells, activation mediated by the presence of multiple binding sites on the target cells. Its three-dimensional structure has been studied by making use of two-dimensional ^{1}H NMR spectroscopy. MCP-3 exhibits the same monomeric structure as the other chemokines, i.e., a three-stranded antiparallel β sheet covered on one face by an α helix. Although it belongs to the same subfamily as RANTES (Chung *et al.*, 1995; Faitbrother *et al.*, 1994) and hMIP-1β (Lodi *et al.*, 1994), the MCP-3 dimer is folded like IL-8 with the so-called $\alpha\beta$ sandwich structural motif. Structural and sequence analysis gives clear indications suggesting that the other MCP chemokines may have the same quaternary structure, contrary to the other β chemokines.

Cytokines form a family of proteins which are produced in the course of immunitary and inflammatory responses and which serve as signal carriers in a dynamic cellular communication network. The chemokine (*chemo*tactic cyto*kine*) subfamily (Brown *et al.*, 1989) is composed of small induced secreted protein, which has a common genomic structure and shares an amino acid sequence homology ranging from 20% to 45% (Oppenheim *et al.*, 1991). This family can be divided into two subfamilies according to the position of cystine residues (Brown *et al.*, 1989): these residues are either separated by one amino acid residue (CXC) (α chemokine family) or are contiguous (CC) (β chemokine family). Mouse lymphotactin (Kelner *et al.*, 1994; Kelner & Zlothnik, 1995; Kennedy *et al.*, 1995) and human SCM-1 (Yoshida *et al.*, 1995) are lymphocyte chemoattractant proteins related to chemokines. However, they possess only the second and the fourth conserved cysteines and may be the first known proteins belonging to a C or γ chemokine subfamily (Kelner *et al.*, 1994). Although chemokines display a wide range of biological activities (Sherry & Cerami, 1991)—including cell-specific chemotaxis and activation, regulation of cell growth, and differentiation, as well as modulation of immune responses—their common pharmacological feature is leukocyte chemoattraction and activation (Brown *et al.*, 1989; Baggiolini *et al.*, 1994; Baggiolini & Dahinden, 1994). They were initially reported to have a strict cellular specificity for neutrophils (α chemokines), for lymphocytes (γ chemokines), or, e.g., for monocytes, basophils, and eosinophils (β chemokines) (Schall, 1991; Sherry & Cerami, 1991; Baggiolini, 1993). Some β chemokines are presently known to have specific receptors on neutrophils. The interaction with these neutrophil receptors has been reported to induce the intracellular calcium release (Baggiolini *et al.*, 1994; Baggiolini & Dahinden, 1994). The chemokine network is then responsible for the communication between different cells in the aspecific response of the immunitary system.

MCP-3[1] (Van Damne *et al.*, 1992; Opdenakker *et al.*, 1993; Minty *et al.*, 1993) was characterized on the basis of its inflammatory and chemotactic activities and its ability to regulate monocytes/macrophages. It has been described to be involved in the activation of a great variety of inflammatory cell types. This activation is mediated by the presence of multiple binding sites on the target cells. MCP-3 is predicted to be able to interact with MCP-1 receptors on monocytes and basophils (Sozzani *et al.*, 1994; Dahinden *et al.*, 1994; Noso *et al.*, 1994; Franci *et al.*, 1995; Combadiere *et al.*, 1995), selective RANTES receptors on basophils and eosinophils (Dahinden *et al.*, 1994; Noso *et al.*, 1994), selective MIP-1α receptors on basophils, eosinophils, and neutrophils (Dahinden *et al.*, 1994), and MIP-1α/RANTES receptors on monocytes (Combadiere *et al.*, 1995; Ben-Baruch *et al.*, 1995).

Several chemokine structures are known thus far: IL-8/NAP-1 (Clore *et al.*, 1990; Baldwin *et al.*, 1991; Clore & Gronenborn, 1991), β-thromboglobulin/NAP-2 (Malkowski *et al.*, 1995), PF-4 (St. Charles *et al.*, 1989; Zhang, X., *et al.*, 1994), and Groα/MGSA (Faitbrother *et al.*, 1994; Kim *et al.*, 1994) as α chemokines and MIP-1β (Lodi *et al.*, 1994) and RANTES (Chung *et al.*, 1995; Skelton *et al.*, 1995) as β chemokines. Here we report the conformational analysis of MCP-3 by two-dimensional ^{1}H NMR spectroscopy. The complete sequential assignment and the tertiary structure in

‡ Coordinates have been deposited in the Brookhaven Protein Data Bank (filename 1NCV).

* To whom correspondence should be addressed. Tel: +33 (4) 91 16 45 35. Fax: +33 (4) 91 16 45 36.

§ AFMB-IFR1, UPR 9039-CNRS.

Present address: Bijvoet Center for Biomolecular Research, Department of Chemistry, Utrecht University, Padualaan 8, NL-3584 CH Utrecht, The Netherlands.

|| SANOFI Recherche.

⊥ SANOFI-Elf Bio Recherche.

⊗ Abstract published in *Advance ACS Abstracts,* March 15, 1997.

[1] Abbreviations: IL-8/NAP-1, interleukin 8/neutrophil activating protein 1 (1il8); MCP-1, monocyte chemoattractant protein 1; MCP-3, monocyte chemoattractant protein 3; MGSA, melanoma growth stimulating activity (1msh; structure **1**); MIP-1α, macrophage inflammatory protein 1α; MIP-1β, macrophage inflammatory protein 1β (1hum); NAP-2, neutrophil activating protein 2 (1nap); NMR, nuclear magnetic resonance; PF-4, platelet factor 4 (1rhp); RANTES, regulated on activation, normal T-cell expressed, and secreted (1rto). In parentheses are given the Brookhaven Data Bank index of the protein structure used for the chemokine comparison.

S0006-2960(96)02792-4 CCC: $14.00

solution are described, and preliminary quaternary structures are proposed, as well as a conformational comparison in terms of structure−function relationships with the other known chemokines.

MATERIALS AND METHODS

Samples. Samples for NMR spectroscopy contain 2 mM CHO-recombinant MCP-3, dissolved in 90% deuterated sodium acetate, 20 mM, and 10% D_2O, at pH 5.

NMR Spectroscopy. Clean total correlation spectra (clean TOCSY) (Griesenger *et al.*, 1988) and nuclear Overhauser effect (NOE) spectra (NOESY) (Jeener *et al.*, 1979; Kumar *et al.*, 1981) were recorded at three temperatures, 290, 295, and 300 K. At 295 and 300 K, the spectra were recorded on an AMX 500 Bruker spectrometer: clean TOCSY, with spin lock times of 60 and 120 ms; NOESY, with a mixing time of 100 ms. The spectral acquisition was done by the pure phase absorption method using the time-proportional phase incrementation (TPPI) method (Marion & Wüthrich, 1983). The water signal was suppressed using a low-power irradiation. At 290 K, spectra were recorded on a DMX 600 Bruker spectrometer: clean TOCSY, with mixing times of 10, 30, 50, 80, and 100 ms; NOESY, with a mixing time of 80 ms. The clean TOCSY were recorded using the TPPI method, using a low-power irradiation to suppress the water signal, while the NOESY spectrum was recorded using the States−TPPI method, using a watergate pulse sequence (Piotto *et al.*, 1992; Sklenar *et al.*, 1993) to suppress the water signal.

Processing. All spectra were processed by NMRPIPE software (Delaglio *et al.*, 1995) on SGI stations. Zero-filling was employed to yield final spectra of 4096 × 2048 data points. The apodization was systematically done by a square sine bell window shifted by 60° with a weighting function in both dimensions F_1 and F_2. After zero-filling, the digital resolution was 3.91 Hz/point in F_1 and 2.2 Hz/point in F_2.

Restraint Collection. The assignment was carried out using the Wüthrich method (Wüthrich, 1986) applied with the EASY software (Eccles *et al.*, 1991) on an IPC SUN station. The spin system identification was obtained by analysis and comparison of clean TOCSY at different mixing times. We failed in recording a useful DQF COSY spectrum, and thus we used a 10 ms clean TOCSY instead. Peaks which are present on this spectrum correspond to only direct correlations. The through-space connectivities were then demonstrated using NOESY spectra. The three recorded temperature allowed us to resolve ambiguities which arise from chemical shift degeneracies.

NOE connectivities, used as input for the structure calculation, were obtained from NOESY spectra recorded in water at different temperatures: they constituted different sets of complementary data. Peaks were integrated by the peak integration routine of the EASY software (Eccles *et al.*, 1991). The calibration curve was obtained after averaging the volume of all resolved peaks used for the calibration: it is based on known distances (d = 1.8 Å between geminal protons; $d_{\alpha N}$ = 2.2 Å in a β strand; $d_{\alpha\alpha(i,j)}$ = 2.3 Å, $d_{\alpha N(i,j)}$ = 3.2 Å, and $d_{NN(i,j)}$ = 3.3 Å between two antiparallel strands of β sheet; d_{NN} = 2.8 Å, $d_{\alpha N(i,i+3)}$ = 3.4 Å, $d_{\alpha N}$ = 3.5 Å, $d_{\alpha N(i,i+4)}$ = 4.2 Å, and $d_{\alpha N(i,i+2)}$ = 4.4 Å in an α helix). Using this curve, we estimated the necessary constant for CALIBA of the DIANA package (Güntert *et al.*, 1991a,b). According to the manually obtained curve, the calculated curve is a function of $1/r^4$. We so obtained a set of restraints with upper limits defined for each volume.

Spin coupling constants $^3J_{HN\alpha}$ were measured with good accuracy on the NOESY 80 ms mixing time recorded at 290 K, using the INFIT routine (Szyperski *et al.*, 1992) from XEASY software. For a given residue, separated NOESY cross-peaks with the backbone amide proton in the $\varpi 2$ dimension were used. Several cross sections through these cross-peaks were selected that exhibit a good signal-to-noise ratio. They were added up, and only those data points of the peak region that were above the noise level were retained. The left and the right ends of the peak region were then brought to zero intensity by a linear baseline correction. After extending the baseline-corrected peak region with zeros on both sides, which is equivalent to oversampling in the time domain, an inverse Fourier transformation was performed. The value of the $^3J_{HN\alpha}$ coupling constant was obtained from the first local minimum. $^3J_{HN\alpha}$ coupling constants were translated into angle restraints using HABAS (Güntert *et al.*, 1989, 1993) from the DIANA package.

Pseudoatom corrections were added when no stereospecific assignment was available (Wüthrich, 1986). Stereospecific assignement was determined either by HABAS (Güntert *et al.*, 1989, 1993), by comparing respective distances involving geminal protons, or by GLOMSA (Güntert *et al.*, 1991a,b), in a back analysis of the previously determined structures in a comparison with the respective distances involving both geminal protons. Both HABAS and GLOMSA are subroutines of the DIANA package (Güntert *et al.*, 1991a,b). Lower distance restraints were systematically set to 1.8 Å. Disulfide bond restraints were used as follows: $d_{C\beta i-S\gamma j} = d_{S\gamma i-C\beta j}$ = 3.1 Å and $d_{S\gamma i-S\gamma j}$ = 2.1 Å. Hydrogen bond restraints were only added in the final steps of refinement, because no exchange data were avalaible; we thus used hydrogen bonds defined by DIANA calculations as being consistent in each calculated structure. Two distance restraints were used to define each hydrogen bond: d_{H-O} = 1.7−2.01 Å and d_{N-O} = 2.7−3.0 Å.

Structure Calculation. Structure calculation was performed by making use of the distance-geometry method (Havel & Wüthrich, 1984; Havel, 1991) with the DIANA package (Güntert *et al.*, 1991a,b). Acceptable structures, in term of distance and angle restraint violations, were energy minimized and then submitted to a molecular dynamic simulation procedure with X-PLOR 3.1 (Brünger, 1992). RMSD (root mean square deviation) and solvent accessibility calculations were also performed by making use of X-PLOR 3.1. Calculations were carried out on HP 9000/715 stations, while graphic analysis was done on SGI stations, by using the TURBO-FRODO software (Roussel & Cambillau, 1989).

A total of 1000 random structures were generated and used in a first round of distance-geometry calculation with only intraresidue and sequential restraints. The analysis of the target function allowed the selection and the introduction of the 500 best structures in a new calculation, using the medium-range restraints. The 250 best structures were then computed with angle and long-range restraints. Successive computations were performed with the complete data set, including at each calculation step the new distance restraints determined from ASNO (Güntert *et al.*, 1989, 1993) of the DIANA package, using the newly recalculated structures. The final calculation was performed after the global stereospecific assignment by making use of GLOMSA (Güntert *et al.*, 1991a,b) of the DIANA package.

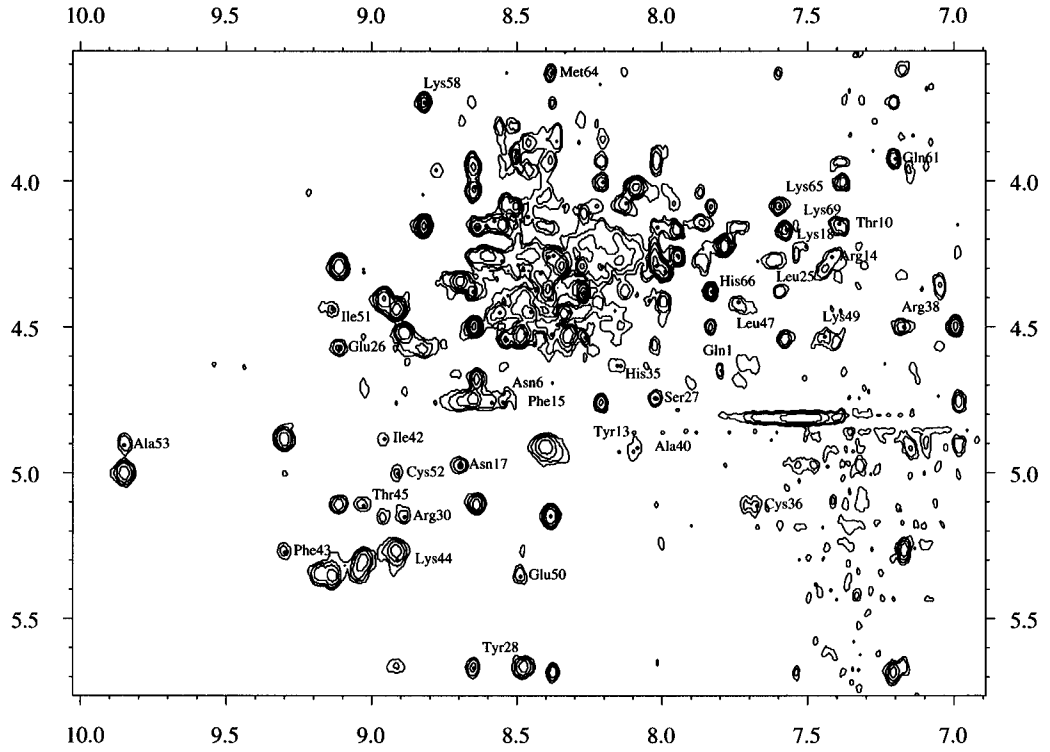

FIGURE 1: Contour plot of the fingerprint region the NOESY spectrum recorded with 80 ms mixing time, at 290 K, pH 5. The Hα/HN cross-peaks of each residue are labeled according to the sequential assignment (except in the overlapped region where they are forbidden to let the figure more readable).

Structures were refined in an AMBER force field and then assessed on the grounds of energy, restraint violations, and deviation from standard protein geometries. We used a slow-cooling molecular dynamic simulation from 4000 to 300 K with 50 K steps. At each temperature step, 50 steps of 0.1 ps each were carried out.

RESULTS AND DISCUSSION

Assignments. The sample was found to be soluble and stable at pH 5.0 and was used over a time period of several months without evidence of degradation. Since biochemical tests determined that MCP-3 is unstable at temperatures over 303 K, spectra were recorded only at low temperatures, i.e., 290, 295, and 300 K.

The spin system assignment was performed using the method described by Wüthrich (1986) and led to nearly full resonance assignment. Spin systems were identified by their characteristic pattern, comparing clean TOCSY 10 ms of mixing time with the other clean TOCSY spectra. The clean TOCSY 10 ms fingerprint consists of 65 well-defined and resolved peaks, added with few low-intensity peaks which can be considered either as remaining HN/Hα correlations from residues located in mobile zones or as probable relayed magnetization between HN and Hβ of serines and threonines. First, NOESY spectra (Figure 1) were used to connect the aromatic spin systems to the aliphatic ones belonging to the same residues. Second, they were used to obtain the sequential assignment which was achieved on the basis of sequential Hα/HN and HN/HN NOE connectivities. The assignment was checked by sequential Hβ/HN connectivities as far as possible (Figure 2). We also measured $^3J_{HN\alpha}$ coupling constants for most of the residues (Figure 2), and we applied the chemical shift index method (Wishart *et al.*, 1992) (Figure 3). Combining the qualitative interpretation of the sequential NOE's, the coupling constants measured from the two-dimensional ^{1}H NOESY 80 ms spectrum at 290 K, and the chemical shift index, elements of secondary structure can be located as follows: three β strands (strand 1, 27−32; strand 2, 40−45; strand 3, 49−54), some indications for an additionnal extended region encompassing residues 14−16, and a C-terminal helix, encompassing residues from 58 to 69. Taking into consideration the nonsequential NOE's involving the backbone resonances of residues in an extended conformation allowed us to determine the sheet organization as an antiparallel β sheet, with an additional three-residue extended zone, located antiparallelly close to strand 3. The β sheet is thus folded as a greek key motif. All prolines (Pro 2, Pro 21, Pro 37, Pro 55, Pro 74) were sequentially connected through strong intensity NOE's between $H\alpha_{i-1}$ and $H\delta_i$ and are thus all in *trans* conformation.

Structure Calculation. Biochemical analysis determined that MCP-3 exists in a monomeric form at low concentrations (Minty, personal communication). The first steps of the NMR analysis were thus done accordingly. A total of 850 NOE's were collected and translated in distance restraints. They consist of 330 intraresidue constraints, 258 sequential constraints, 108 medium-range constraints (33 $i,i+2$; 50 $i,i+3$; 25 $i,i+4$), and 154 long-range constraints. In addition, 55 $^3J_{HN\alpha}$ coupling constants were collected from a NOESY 80 ms spectrum and were translated in angle restraints; 16 (10%) geminal protons were also stereospecifically assigned. No amide hydrogen-exchange experiments were recorded because of instability during the lyophilization. During distance-geometry calculation steps, 14 hydrogen bonds were identified which were consistent in each structure. Accordingly, they have afterward been used in the calculation as distance restraints.

During the sequential assignment, the hypothesis of a dimeric quaternary structure was postulated: unambiguous restraints were found between the first and last residues

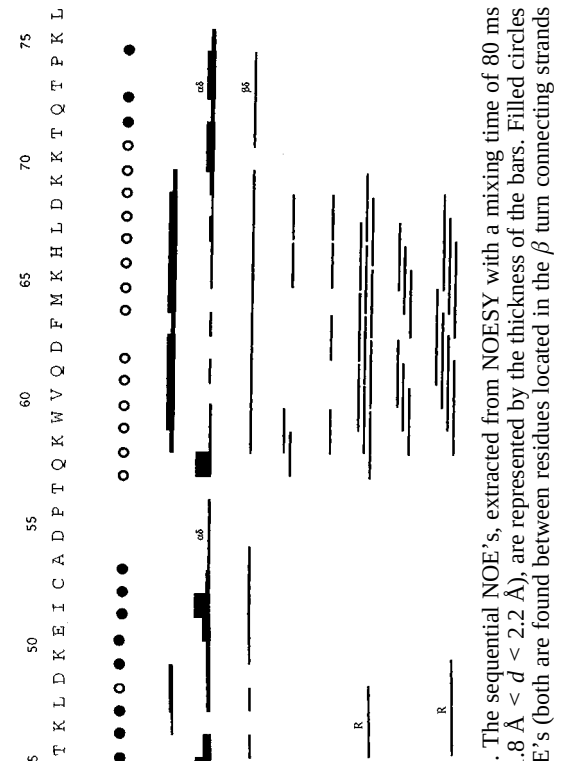

FIGURE 2: Amino acid sequence of MCP-3 and survey of NMR data used for locating the secondary structure elements. The sequential NOE's, extracted from NOESY with a mixing time of 80 ms and classified as very weak (1.8 Å < d < 5 Å), weak (1.8 Å < d < 3.5 Å), medium (1.8 Å < d < 2.8 Å), and strong (1.8 Å < d < 2.2 Å), are represented by the thickness of the bars. Filled circles represent $^3J_{HN\alpha}$ coupling constants greater than 6.0 Hz and open circles those less than 6.0 Hz. R indicates reverse NOE's (both are found between residues located in the β turn connecting strands 2 and 3 and are due to the particular conformation of this turn).

belonging to the same strand of the β sheet. This hypothesis allowed the assignment of additional unambiguous NOE's. The new data set consists of 1720 constraints [850 per monomer, implemented with 20 intermonomeric restraints (Table 1), 16 experimental restraints and 4 consistent hydrogen bonds]. The distance-geometry calculation of the dimer was independently performed following the same strategy used for the monomer calculation, except that we used only 100 initial structures. The NOE's used for the final dimer calculation are summarized in a contact diagram (Figure 4).

The 24 lower energy monomer structures and the 9 lower energy dimer structures were then refined and energy minimized down to convergence. Cα tracing of monomer superposition is shown in Figure 5, as well as views of the lowest energy monomer and dimer structures (Figure 6). Statistics of both final structure families are summarized in Table 2. By analyzing the distribution of the restraints and the RMSD curve for each residue (Figure 7), we observe that the distribution is standard: extended zones are defined by long-range restraints and helix zones by medium-range restraints. Moreover, many restraints describe the secondary structures, while loop regions are featured by a low number of restraints per residue. This difference may perhaps explain the RMSD obtained when we superimposed the structure family on the average structure: it is about 4 Å, despite the high average number of restraints per residue (13.5).

Description of the Structure. The shape of the MCP-3 monomer is that of an elongated tetrahedral. It consists of a three-stranded antiparallel β sheet and a three turn C-terminal α helix lying above the sheet floor. The N-terminal extremity is disordered up to residue 12, but located close to the helix; it consists of a long mobile loop, spatially stabilized because of the two disulfide bonds which link Cys 11 with Cys 36 and Cys 12 with Cys 52. Both disulfide bonds adopt a left-handed conformation. This first loop is followed by a five-residue extended zone (residues 12−16). Residues from 17 to 26 form the second loop, connecting this extended zone to strand 1. The first residue (Ser 27) of strand 1 seems to be disordered, with a strong HN/HN NOE between residues 26 and 27, together with a low $^3J_{HN\alpha}$ coupling constant for residue 27. Actually, Ser 27 adopts a twisted conformation and its amide proton shares the carbonyl of Lys 44 as hydrogen bond acceptor with the amide proton of Glu 26. A third loop exists between strand 1 and strand 2: it runs from residue 33 to residue 39. The turn between strand 2 and strand 3 (residues 45−49) is folded as a five-residue hairpin loop with a type I β turn and a standard β bulge (Richardson, 1981; Sibanda & Thornton, 1985). Strand 3 and the α helix are connected together through a hairpin running from residues 54 to 57. The C-terminal extremity is highly mobile from residue 70 to the end. The α helix is packed close to the β sheet, especially through an important number of NOE's between hydrophobic residues of the β sheet (Tyr 28, Val 41, Phe 43, Ile 51, Ala 53) and of the α helix (Trp 59, Val 60, Phe 63, Leu 67). The helix axis is roughly orthogonal to the sheet axis, taking into account the mobility of the helix due to the flexible turn connecting the helix to the sheet.

The MCP-3 dimer is globular. The dimer interface is made of strand 1 antiparallel to itself. The interface is determined on the basis of 16 unambiguous NOE's, and after the first refinement steps, four hydrogen bonds were defined as being consistent between the two monomers. Restraints

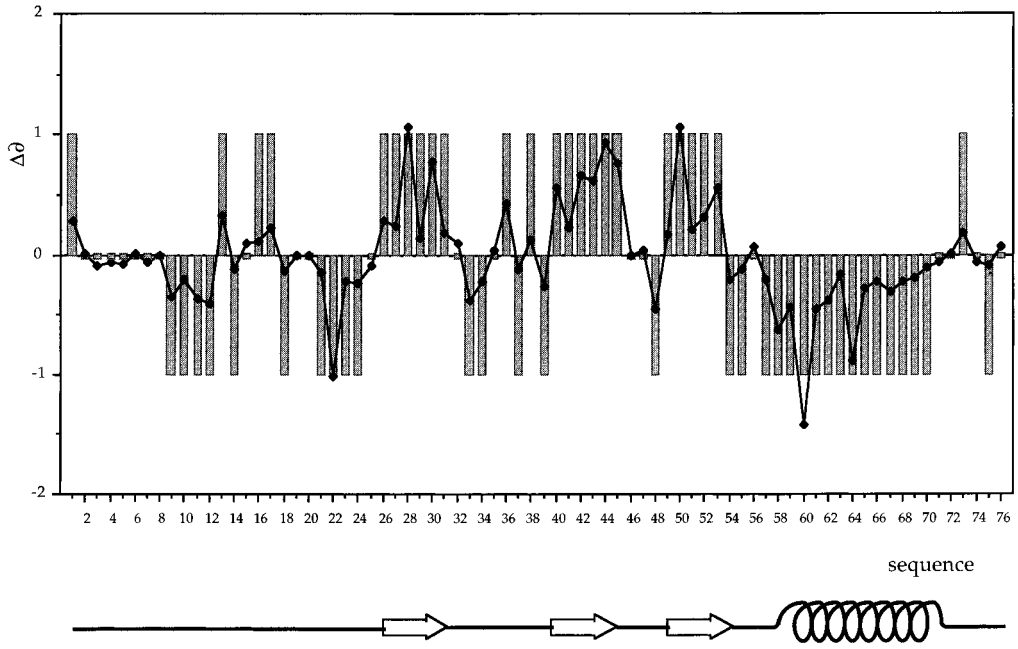

FIGURE 3: Chemical shift analysis of Hα protons. Filled diamond shapes and curve represent calculated chemical shift variation from the standard chemical shifts. Gray bars represent the chemical shift index as defined by Wishart (1992).

Table 1: Intermonomeric Restraints Used in the Structure Calculation of the Dimeric Structure Family[a]

experimental restraints		hydrogen bonds	
HN Leu 17	HN Lys 75′	Tyr 28 HN	O Arg 30′
HN Leu 25	Hα Ser 34′	Arg 30 HN	O Tyr 28′
HN Tyr 28	HN Arg 30′		
Hα Ser 27	Hα Thr 31′		
HN Tyr 28	Hα Thr 31′		
NηH$_2$ Arg 30	Hβ Asp 68′		
HN Glu 39	HN Thr 71′		
Hϵ1 Trp 59	Hβ Lys 75′		

[a] Hydrogen bonds were used as restraints only in the last refinement calculation step.

between monomers are essentially located between strands 1 and 1′, but we also found NOE's between HN of Asn 17 and HN of Lys 75′, HN of Leu 25 and Hα of Ser 34′, NηH$_2$ of Arg 30 and Hβ of Asp 68′, HN of Glu 39 and HN of Thr 71′, and Hϵ1 of Trp 59 and Hβ of Lys 75′ (Figure 7). The hydrogen bonds later used in the structure calculations are between HN of Tyr 28 and O of Arg 30′ and HN of Arg 30 and O of Tyr 28′. Monomer structures are identical, within experimental error and loop mobility, due to the independent refinement of each monomer. MCP-3 dimerizes according to a 2-fold rotation axis, centered between residues 29 of each monomer. Because of the dimerization, the β sheet consists now of an eight-stranded β sheet, which is covered on one side by the two antiparallel helices. The five-residue extended zone is connected to strand 3 by one hydrogen bond involving HN of Cys 52 and O of Arg 14 and forms thus a real fourth strand. The β sheet consists of eight antiparallel β strands organized onto the monomer structure as a $(4,0)_N$ greek key-type β sheet (Hutchinson & Thornton, 1993), with a three turn C-terminal α helix lying above the sheet floor: it is a closed $\alpha\beta$ sandwich. The helices, approximately separated by 10.5 Å from axis to axis, are now stabilized and form an angle of 80° with the sheet axis.

Hydrophobicity analysis clearly indicates that the MCP-3 monomeric structure is not stable, contrary to the MCP-3 dimer. In the monomeric structure, the proteic core is actually exposed to the solvent. In Figure 8 are shown the

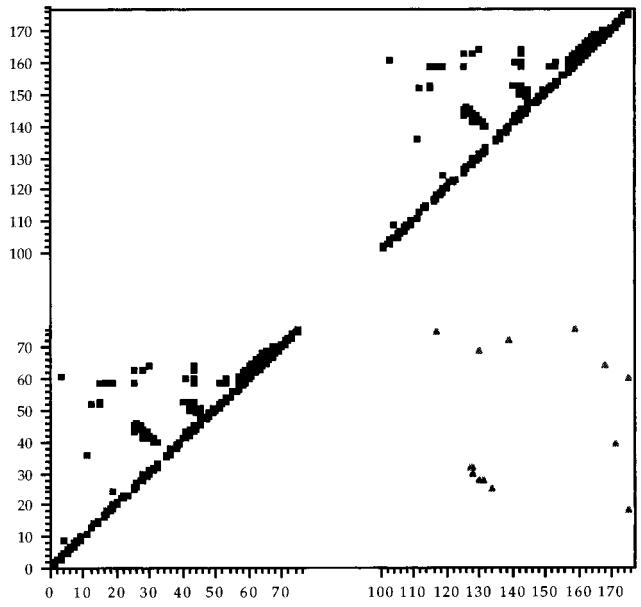

FIGURE 4: Summary of NOE data used for the structure calculation. Monomer 1 is numbered from 1 to 76, and monomer 2 is numbered from 101 to 176. Filled squares above the diagonal represent intramonomeric restraints, while filled triangles below the diagonal represent intermonomeric restraints.

backbone and side chain accessibilities for each residue in the monomeric and dimeric structure. The hydrophobic residues Pro 2, Gly 4, Phe 15, Ile 16, Pro 21, Leu 25, Tyr 28, Pro 55, and Leu 67, which are exposed in the MCP-3 monomer, are buried in the MCP-3 dimer. The dimerization would thus allow to shield from the solvent the large hydrophobic surface. That results in a large interface surface of about 800 ± 65 Å^2. The hydrophobic contacts between the helix and the sheet are responsible for their relative orientation. There is a close packing of Val 3, Phe 15, Leu 25, Tyr 28, Val 41, Phe 43, Ile 51, Ala 53, Pro 55, Trp 59, Val 60, Phe 63, and Leu 67 (Figure 9).

Val 60 exhibits upfield chemical shifts (compared to standard chemical shifts) for each of its protons: $\Delta\delta$[HN]

FIGURE 5: Cα tracing of the 24 best structures of the monomer family. The structures are represented and colored using secondary structure standard colors: in blue, β strands, in red, α helices, and in yellow, loops and turns.

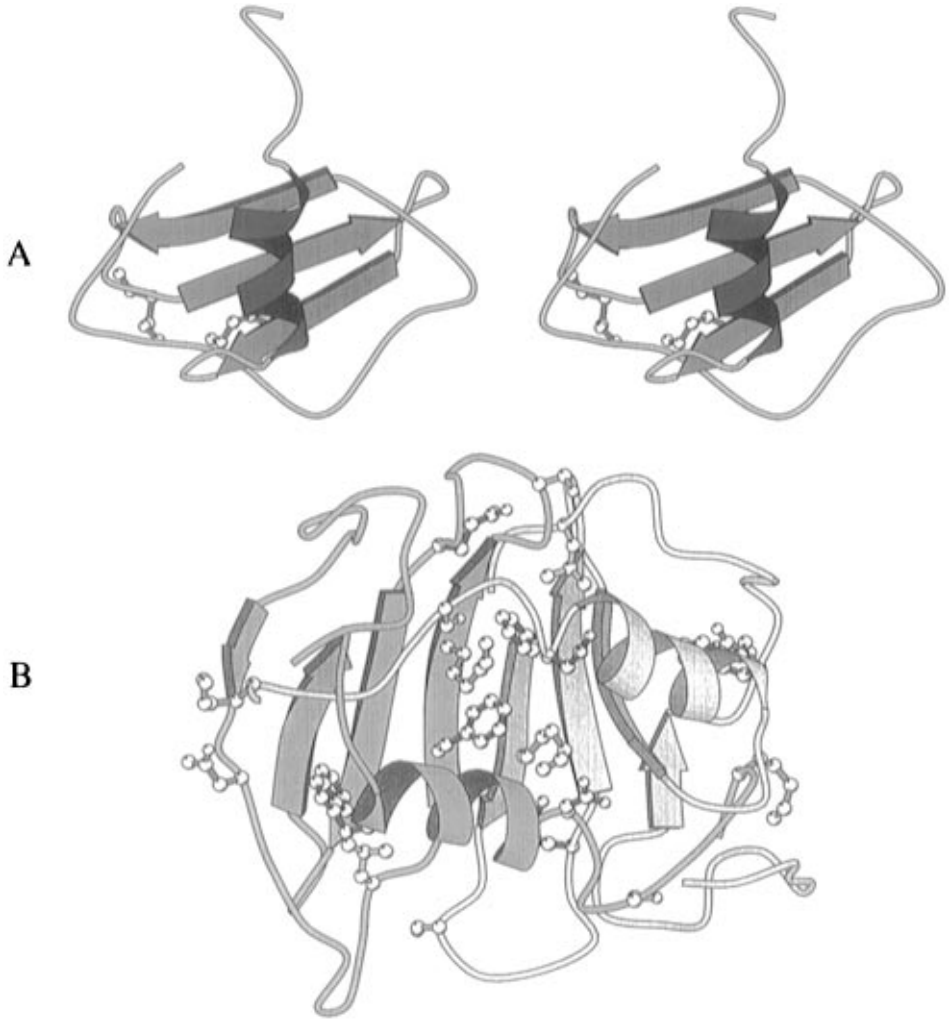

FIGURE 6: (A) Molscript (Kraulis, 1991) stereo ribbon drawing of the lowest energy structure of the monomer, with the disulfide bridge represented in green balls and sticks. (B) Molscript ribbon drawing with side chains of residues involved in intermonomeric restraints. Each monomer main chain is shown in a different color, and side chains are colored in standard residue type color.

$= -2.758$ ppm, $\Delta\delta[H\alpha] = -1.426$ ppm, $\Delta\delta[H\beta] = -0.382$ ppm, and $\Delta\delta[C\gamma H_3] = -0.588$ and -1.72 ppm. This is due to its location nearby Tyr 28, Phe 43, Trp 59, and Phe 63 from each monomer, which create a strong ring current field in the environment of Val 60.

Comparison with the Synthetic MCP-3 Structure. Recently, Kim *et al.* (1996) reported the NMR structure of synthetic MCP-3. Surprisingly, they found out that it is in a monomeric form. The three-dimensional structure of this monomeric form perfectly superimposes on that of the monomer we described; i.e., it is composed by a three-stranded antiparallel β sheet with a C-terminal α helix crossing over the β sheet. Despite this homology, the authors gave evidence indicating that synthetic MCP-3 does not have the propensity to dimerize and remains a monomer under a wide range of conditions.

Table 2: Structural Statistics of Both Structure Families[a]

	$\langle DG_{mono} \rangle$	$\overline{DG}_{mono}$	$\langle DG_{di} \rangle$	$\overline{DG}_{di}$
NOE violation >0.2 Å	0	0	0	0
RMSD (Å)				
bonds	0.025 ± 0.0006	0.023	0.025 ± 0.003	0.028
angles	4.5 ± 0.2	6.04	8.694 ± 0.327	6.09
impropers	0.81 ± 0.05	0.7154	0.873 ± 0.105	0.6387
dihedrals	15 ± 0.5	21.338	14.667 ± 0.497	22.215
torsion angles	51.4 ± 2.8	46.665	51.167 ± 1.627	53.9808
NOE	0.017 ± 0.001	0.014	0.014 ± 0.001	0.013
backbone	4.076		3.541	
all heavy atoms	4.554		4.101	
secondary structures	0.951		1.560	

[a] $\langle DG_* \rangle$ are the final structures obtained by distance geometry and slow cooling simulation refinement. $\overline{DG}_*$ is the mean structure obtained by averaging the coordinates of the individual DG structures.

In our hands, the NOESY spectra complexity (Figure 1), as well as several unambiguous NOE's, cannot be explained simply by assuming a monomeric structure. Furthermore, either at temperatures higher than 300 K, or at pH below 5, solubility problems are encountered: generally speaking the recombinant MCP-3 is poorly soluble and has a strong tendency to aggregate. In addition, it was also impossible to solubilize MCP-3 after lyophilization. All these arguments, as well as the ones above-described, strongly indicate that recombinant MCP-3 exists as a dimeric form in highly concentrated solutions.

Comparison with Other Chemokines. The superimposition of the MCP-3 monomer onto all the other known chemokine structures (β chemokines as well as α chemokines) clearly indicates that chemokines share a common topology, despite the differences arising from mutations, deletions, and insertions (Figure 10). All the monomers consist of a three-stranded antiparallel β sheet covered on one face by an α helix. Nevertheless, a few structural differences between the structures can be observed: structural discrepancies are essentially located on the N- and C-terminal extremities, which adopt different orientations in the different molecules.

In Figure 11 is shown a multiple sequence alignment among all the available chemokine sequences. Beyond the conserved cystines characteristic of the chemokine family, a few conservative substitutions are observed within the family. They concern residues Tyr 13, Ile 20, Leu 25, Tyr 28, Val 41, Ile 42, Phe 43, Ile 51, Ala 53, and Val 60. By analyzing independently CC and CXC chemokine subfamilies, several other strictly conserved residues are identified. They consist of residues Tyr 28, Val 41, Phe 43, Thr 45, Lys 46, Ala 53, Trp 59, Val 60, and Leu 67 in the CC subfamily and of residues Leu 5, Thr 12, Pro 16, Ile 22, Val 27, Gly 31, His 33, Leu 43, Leu 51, and Leu 66 (according to the IL-8 numbering) in the case of CXC chemokines. In both cases these residues are essentially located in or in proximity of the β sheet. No strictly conserved residues are found in the helix. Nevertheless, the hydrophobic character of the helix is retained by means of conservative substitutions.

Considering conserved and packed residues, it is clear that the monomer structure similarity between the chemokines arises from the primary structure. A comparative analysis of three-dimensional structures of IL-8 (Clore *et al.*, 1990; Baldwin *et al.*, 1991; Clore & Gronenborn, 1991) and hMIP-1β (Lodi *et al.*, 1994) (representing respectively α and β chemokines) allowed to determine a general rule for the chemokine dimerization (Covell *et al.*, 1994; Clore & Gronenborn, 1995): a few conserved residues, characteristic of each of the chemokine subfamilies, are involved in dimer stabilization or destabilization. In MCP-3, the involved residues are Tyr 28 (strand 1), Arg 30 (strand 1), and Asp 68 (helix). Upon $\alpha\beta$ sandwich-type dimerization, these residues are in close contact to one of the others in each monomer. The guanidinium group of Arg 30 interacts with the carboxyl group of Asp 68′ through a salt bridge. It also exists an hydrogen bond between NϵH of Arg 30 and either the hydroxyl group of Tyr 28′ or the carboxyl group of Asp 68′ (Figure 12). Moreover, in these polar interactions, it occurs a hydrophobic contact between the aromatic ring of Tyr 28 and one methyl group of Leu 67′.

This quaternary organization may also be found in MCP-1 and MCP-2: the tyrosine, the arginine, and the leucine are conserved, as well as the aspartate, except in mouse MCP-1 in which it is replaced by a threonine. Aspartate and threonine have approximately the same steric hindrance, and the hydroxyl group of threonine may form a stabilizing interaction with the arginine. In other β chemokines, arginine and aspartate are replaced by either residues which have an identical polarity (asparagine−arginine, glutamate−glutamate, tyrosine−glutamate) or residues having a larger overall steric hindrance and which are thus unable to stabilize the $\alpha\beta$ sandwich dimer type. The structures of two β chemokines are known thus far [hMIP-1b (Lodi *et al.*, 1994) and RANTES (Chung *et al.*, 1995; Faitbrother *et al.*, 1994)], and their quaternary structure is described as bean type with α helices being located on each side of the molecule. MCP chemokines may thus be considered as a subfamily within the β chemokine family (Proost *et al.*, 1996).

Structure−Function Relationships. Among chemokines, MCP-1 is the member which shares the highest extent of homology with MCP-3. The relationships between structure and activity were elucidated for MCP-1 by site-directed mutagenesis (Zhang, Y. J., *et al.*, 1994). This study was aimed at determining which residues were involved in monocyte chemotaxis. Differents parts of the molecule, which had already been expected to be involved in the activity, were specifically mutated (Tanaka *et al.*, 1988; Beall *et al.*, 1992). Accordingly, the residues playing a crucial role in activity could be identified. On the basis of the high homology between MCP-1 and MCP-3 (77%), the functional residues can be assumed to be the same. Moreover, MCP-3 interacts with MCP-1 receptor C-C CKR-2A and -B. The N-terminal region was found to be required for the activity, expecially Asp 3. However, upon introduction of a charged residue at any other position in the N-terminus, except position 6, the activity could be restored. Tyr 28 and Arg 30 are crucial for the chemotactic activity. This is consistent with the ability of a peptide consisting of residues 13−35 to compete with MCP-1 and to have chemoattractant activity (Valente *et al.*, 1991). Moreover, Zhang *et al.* reported that Arg 24 is involved in the interactions with the receptor, since a mutation of this residue drastically reduced monocyte chemoattractant activity. Mutations in the C-terminal part, expecially if located in the helices, decrease the monocyte chemotactic power of MCP-1. Asp 68 was also described to be involved in the activity.

All the residues described by Zhang *et al.* are conserved in the MCP-3 sequence, except for Asp 3 which is replaced

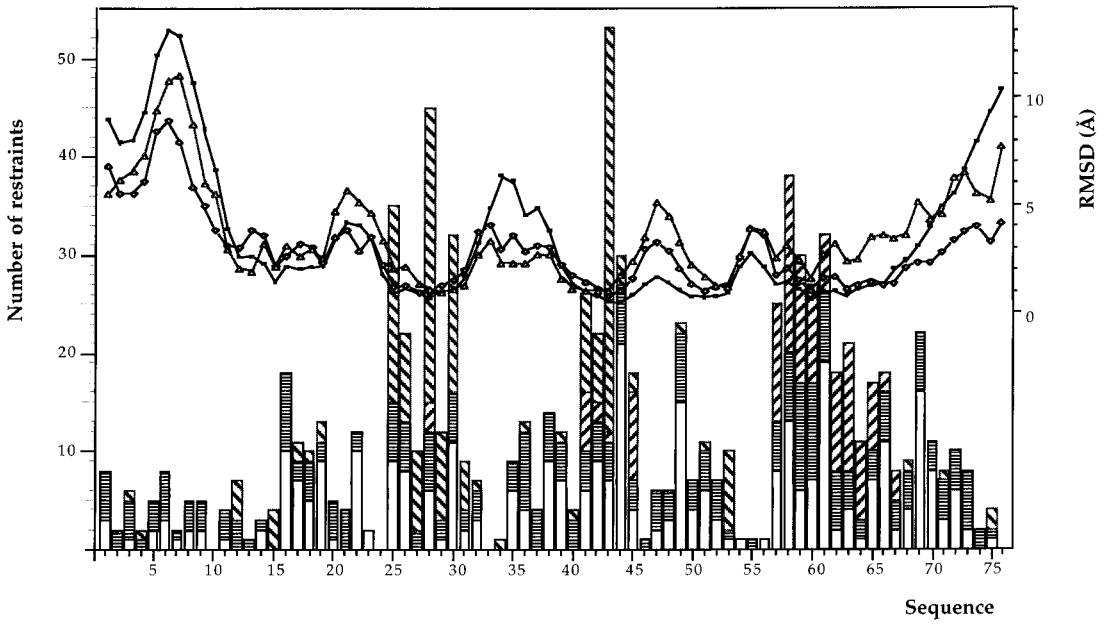

FIGURE 7: Number of restraints and RMSD curve for each residue of the sequence. Sequential, medium-range, and long-range restraints are shown twice (once for each residue it connects). ◹ indicates intraresidue, ◪ sequential, ■ medium-range and □ long-range restraints. RMSD is calculated by superimposition of structure family and their average structure: −■− is the RMSD curve of the monomer structure, −◇−, the monomer A RMSD curve of the dimer structure, and −△−, the monomer B RMSD curve of the dimer structure.

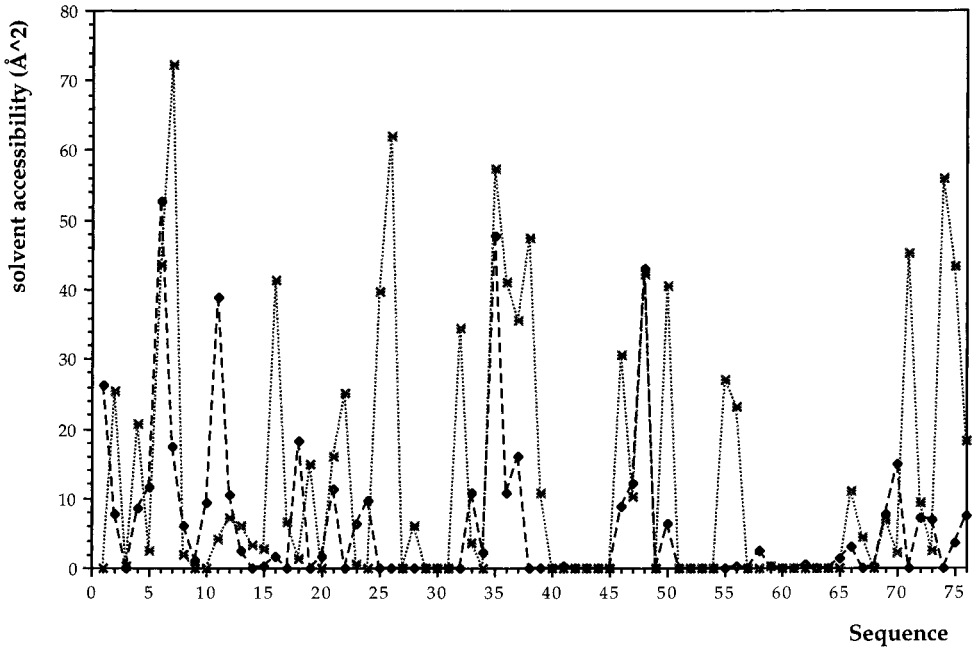

FIGURE 8: Solvent accessibility for the backbone of each residue in both the monomer (···×···) and (- -◆- -) dimer structure. For the dimer, accessibility values for each monomer are averaged.

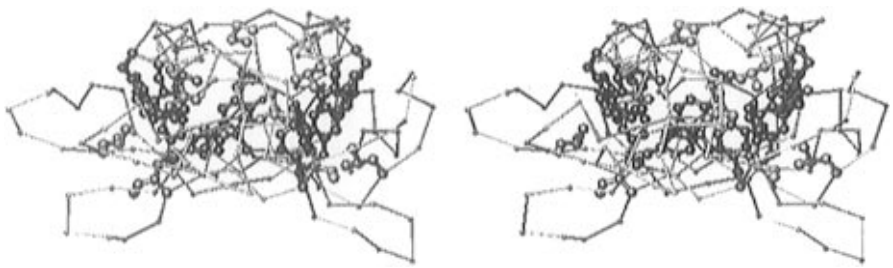

FIGURE 9: Stereoview of the Cα tracing of the average minimized dimer structure with aromatic (purple) and hydrophobic aliphatic (yellow) residues involved in the relative orientation of the helix in regard with the sheet.

by a valine. Furthermore, no charged residue occurs in the neighborhoods. Moreover, in MCP-3, Val 3 is buried in the hydrophobic close packing. Indications on the MCP-3 counterpart of Asp 3 are expected to be provided by site-directed mutagenesis experiments on MCP-3. Residues Tyr 28 and Arg 30, being located in a cleft defined by the two

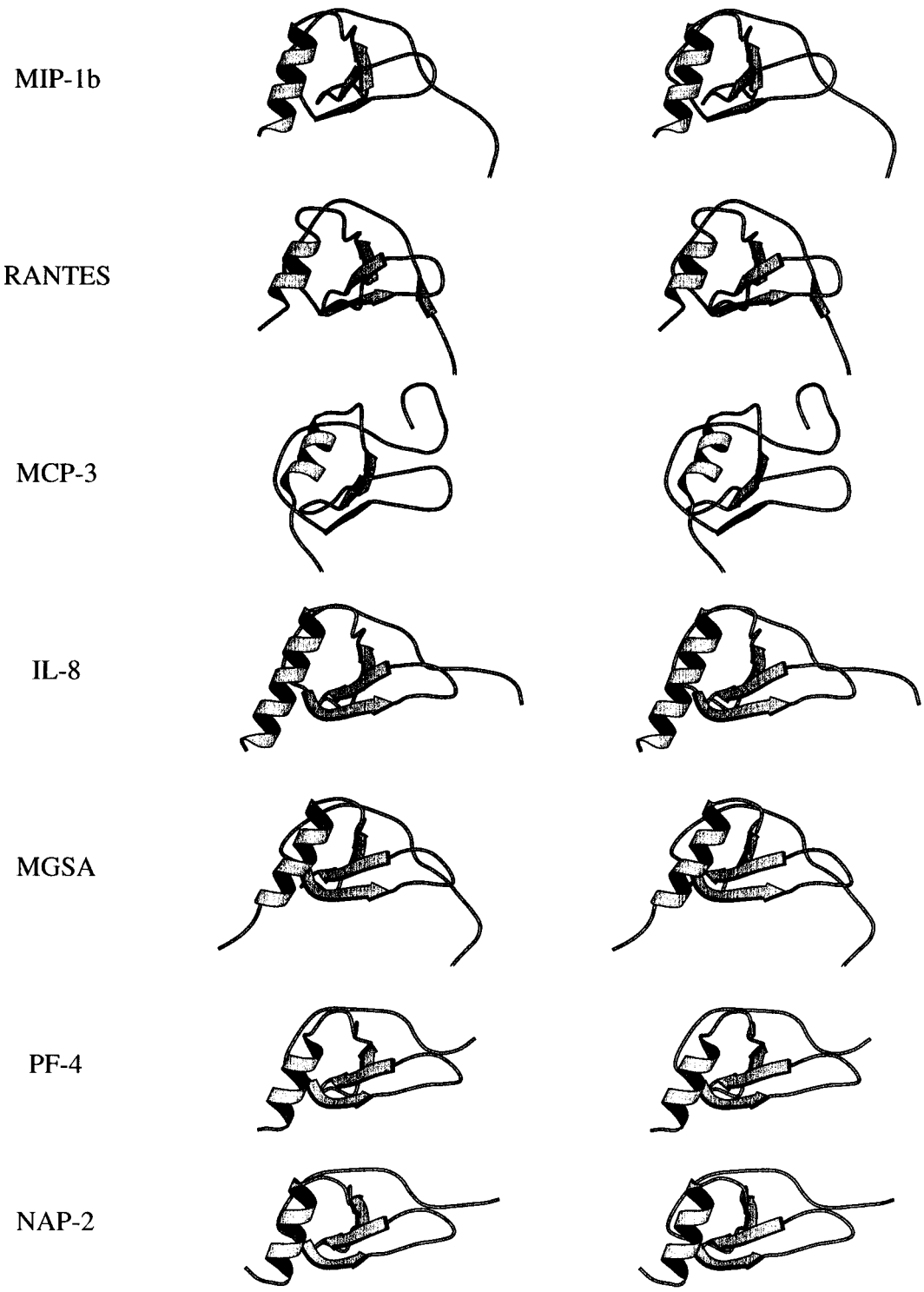

FIGURE 10: Molscript stereo ribbon drawing of seven chemokine monomers: MIP-1β (Lodi *et al.*, 1994), RANTES (Chung *et al.*, 1995; Skelton *et al.*, 1995), IL-8 (Clore *et al.*, 1990; Baldwin *et al.*, 1991; Clore & Gronenborn, 1991), MGSA/Groα (Faitbrother *et al.*, 1994; Kim *et al.*, 1994), PF-4 (St. Charles *et al.*, 1989; Zhang, X., *et al.*, 1994), and NAP-2 (Malkowski *et al.*, 1995).

helices, are not accessible to the solvent. Although Arg 24 points toward the helices, it is nevertheless accessible to the solvent. Asp 68 is located in the C-terminal part of the helices and is in close interaction with Arg 30. Nevertheless, these residues, except the Arg 24, are partially buried, and the Asp 68 is oriented toward the β sheet. They are thus not accessible to the receptor. In order to allow the above-mentionned residues to interact with the receptor, a conformational rearrangement of the helices should be invoked. This conformational change would occur upon interaction with the receptor and would cause the two helices to move away from each other. This rearrangement would consist at the same time of a translation and a rotation, allowing the exposition of the helix side containing the Asp 68.

Conclusion. Two types of dimerization in the chemokine subfamily are described thus far, i.e., IL-8 type and hMIP-1β type. Residues of IL-8 involved in the binding of the receptor would participate in intermolecular interface contacts in the hMIP-1β dimer: it is not yet clear whether chemokines act as monomers or dimers when interacting with their receptor (Clark-Lewis *et al.*, 1991; Herbert *et al.*, 1991; Gayle *et al.*, 1993; Moser *et al.*, 1993; Clubb *et al.*, 1994). The

Chemokines α:

huIL-8 SAKELR**C**Q**C**IKTYSKPFHPKFIKELRVIESGPH**C**ANTEIIVKLS.DGREL**C**LDPKENWVQRVVEKFLKRAENS
pigIL-8 SA.ELR**C**Q**C**INTHSTPFHPKFIKELRVIESGPH**C**ENSEIIVKLV.NGKEV**C**LDPKEKWVQKVVQIFLKRTEKQQQQQ
rabIL-8 IGTELR**C**Q**C**IKTHSTPFHPKFIKELRVIESGPH**C**ANSEIIVKLV.DGREL**C**LDPKEKWVQKVVQIFLKRAEQQES
huGroα/MGSA ASVATELR**C**Q**C**LQTLQG.IHPKNIQSVNVKSPGPH**C**AQTEVIATLK.NGRKA**C**LNPASPIVKKIIEKMLNSDKSN
huGroβ/huMIP-2α APLATELR**C**Q**C**LQTLQG.IHLKNIQSVKVKSPGPH**C**QTEVIATLKK.NGQKA**C**LNPASPMVKKIIEKMLKNGKSN
huGroγ/huMIP-2β ASVVTELR**C**Q**C**LQTLQG.IHLKNIQSVNVRSPGPH**C**AQTEVIATLK.NGKKA**C**LNPASPMVQKIIEKILNKGSTN
moMIP-2 AVVASELR**C**Q**C**LKTLPR.VDFKNIQSLSVTPPGPH**C**AQTEVIATLK.GGQKV**C**LDPEAPLVQKIIQKILNKGKAN
ratMIP-2 VVVASELR**C**Q**C**LTTLPR.VDFKNIQSLTVTPPGPH**C**AQTEVIATLK.DGHEV**C**LNPEAPLVQRIVQKILNKGKAN
huNAP-2 AELR**C**M**C**IKTTSG.IHPKNIQSLEVIGKGTH**C**NQVEVIATLK.DGRKI**C**LDPDAPRIKKIVQKKLAGDESAD
boPF-4 …EGGEDEDLQ**C**V**C**LKTTSG.INPRHISSLEVIGAGTH**C**PSPQLLAT.KKTGRKI**C**LDQQRPLYKKILKKLLDGDES
huPF-4 EAEEDGDLQ**C**L**C**VKTTSQ.VRPRHITSLEVIKAGPH**C**PTAQLIATLK.NGRKI**C**LDLQAPLYKKIIKKLLES

Chemokines β:

boMCP-1 QPDAINSQVA**C**.**C**YTFNSKKISMQRLMNYRRVTSSK.**C**PKEAVIFKTIL.GKEL**C**ADPKQKWVQDSINYLNKKNQTPKP
huMCP-1 QPDAINAPVT**C**.**C**YNFTNRKISVQRLASYRRITSSK.**C**PKEAVIFKTIV.AKEI**C**ADPKQKWVQDSMDHLDKQTQTP
moMCP-1/mJE QPDAVNAPLT**C**.**C**YSFTSKMIPMSRLESYKRITSSR.**C**PKEAVVFVTKL.KREV**C**ADPKKEWVQTYIKNLDRNQMRSEPT…
ratMCP-1 QPDAVNSPVT**C**.**C**YTFTNKTISVKRLMSYRRINSTK.**C**PKEAVIFMTKL.AKGI**C**ADPKQKWVQDAIANLDKKMQTPKTL…
huMCP-2 QPDSVSIPIT**C**.**C**FNVINRKIPIQRLESYTRITNIQ.**C**PKEAVIFKTKR.GKEV**C**ADPKERWVRDSMKHLDQIFQNL
huMCP-3 QPVGINTSTT**C**.**C**YRFINKKIPKQRLESYRRTTSSH.**C**PREAVIFKTKL.DKEI**C**ADPTQKWVQDFMKHLDKKTQTPKL
huI-309 KSMQVPFSR**C**.**C**FSFAEQEIPLRAILCYRN.TSSI.**C**SNEGLIFKLKR.GKEA**C**ALDTVGWVQRHRKMLRHCPSKRK
huRANTES SPYSSD.TTP**C**.**C**FAYIARPLPRAHIKEYFY.TSGK.**C**SNPAVVFVTKR.NRQV**C**ANPEKKWVREYINSLEMS
moRANTES SPYGSD.TTP**C**.**C**FAYLSLALPRAHVKEYFY.TSSK.**C**SNLAVVFVTRR.NRQV**C**ANPEKKWVQEYINYLEMS
huLD78β APLAADTPTA**C**.**C**FSYTSRQIPQNFIADYFE.TSSQ.**C**SKPSVIFLTKR.GRQV**C**ADPSEEWVQKYVSDLELSA
huLD78/huMIP-1α ASLAADTPTA**C**.**C**FSYTSRQIPQNFIADYFE.TSSQ.**C**SKPGVIFLTKR.SRQV**C**ADPSEEWVQKYVSDLELSA
moMIP-1α APYGADTPTA**C**.**C**FSY.SRKIPRQFIVDYFE.TSSL.**C**SQPGVIFLTKR.NRQI**C**ADSKETWVQEYITDLELNA
huMIP-1β APMGSDPPTA**C**.**C**FSYTARKLPRNFVVDYYE.TSSL.**C**SQPAVVFQTKR.SKQV**C**ADPSESWVQEYVYDLELN
moMIP-1β APMGSDPPTS**C**.**C**FSYTSRQLHRSFVMDYYE.TSSL.**C**SKPAVVFLTKR.GRQI**C**PNPSQPWVTEYMSHLELN
huG-26 SAPMGSDPPTA**C**.**C**FSYTARKLPRNFVVDYYE.TSIL.**C**SQPAVVFQTKR.SKQV**C**ADPSETWVQEYVYDLELN

Chemokines γ:

moLymphotactin EGVGTEVLEESS..**C**VNLQTQRLPVQKIKTYIIW.EG...AMRAVIFVTKR.GLKI**C**ADPEAKWVLAAIKTVDGRASTRKNMA…
huSCM-1 EGVGSEVSDKRT..**C**VSLTTQRLPVSRIKTYTI.TEGS...LRAVIFITKR.GLKV**C**ADPQATWVRDVVRSMDRKSNTRNNMA…

FIGURE 11: Sequence alignment of a few chemokine primary structures. Conserved cysteines are in bold characters.

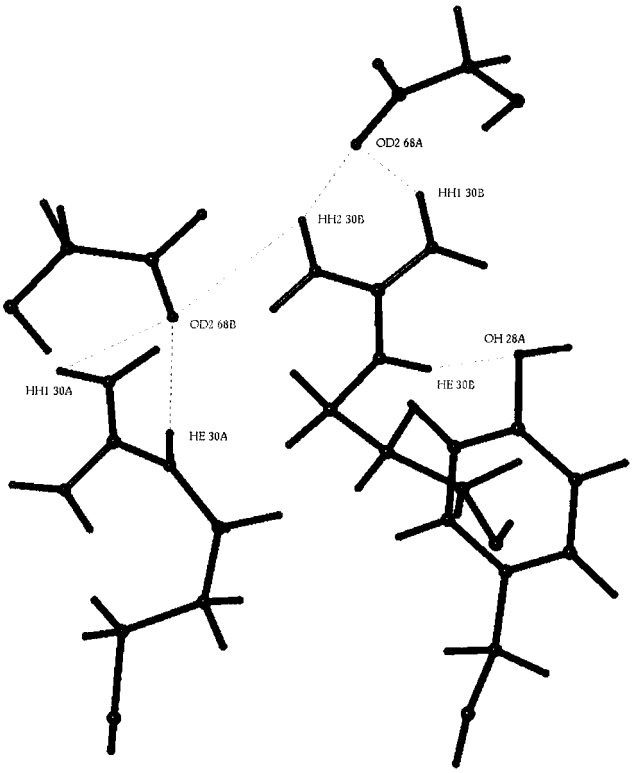

FIGURE 12: Polar stabilizing interactions between monomers in the MCP-3 dimer between residues Tyr 28, Arg 30 and Arg 30′, and Asp 68 and Asp 68′.

circulating concentration of chemokines (in the nanomolar range) is well below the equilibrium constant of dimerization so that circulating chemokines would be monomeric under physiological conditions (Burrows *et al.*, 1994; Paolini *et al.*, 1994). The monomeric form was shown to be fully active in leukocyte chemoattraction and activation (Rajarthnam *et al.*, 1994). However, there are strong indications that the chemokines act also in an immobilized form bound to the endothelial surface, thereby preventing the soluble chemokines from being rapidly washed away *in vivo* and permitting the formation of a chemokine concentration gradient through which the effector cells can migrate (Tanaka *et al.*, 1993). In this way, the local concentration of chemokine would be high, and the dimeric form would then predominate. Beyond hMIP-1β, RANTES has a hMIP-1β dimer type (both CC chemokines), and beyond IL-8, chemokines having a IL-8 dimer type are PF-4, NAP-2, MGSA/Groα (all CXC chemokines) and MCP-3 (CC chemokines). While leukocyte specificity is coded in the primary structure, the formation of a stable dimer requires the presence of a specific cluster of residues on the surface of the monomer, able to form a complementary dimer interface.

NOTE ADDED IN PROOF

An X-ray structure of MCP-1 has recently been published (Lubkowski *et al.*, 1997) describing two crystal forms. In the P form, the standard CC chemokine dimer has been found, while in the I form, a second mode of association, identical to the one herein described, has been described in the I form.

ACKNOWLEDGMENT

We thank Pr. G. Otting for spectral recording, Dr. K. D. Berndt for helpful discussion about software and work strategy, Dr. F. Delaglio for sending us NMRpipe software, and E. Blanc and Dr. M. Czjzek for scientific discussions as well as Dr. S. Longhi for careful reading of the manuscript.

SUPPORTING INFORMATION AVAILABLE

^{1}H chemical shift assignments of MCP-3 at 17 °C, pH 5.0 (4 pages). Ordering information is given on any current masthead page.

REFERENCES

Baggiolini, M. (1993) *Clin. Invest. 71*, 812−814.

Baggiolini, M., & Dahinden, C. A. (1994) *Immunol. Today 15*, 127−133.
Baggiolini, M., Dewald, B., & Moser, B. (1994) *Adv. Immunol. 55*, 97−179.
Baldwin, E. T., Weber, I. T., St. Charles, R., Xuan, J.-C., Appella, E., Yamada, M., Matsushima, K., Edwards, B. F. P., Clore, G. M., Gronenborn, A. M., & Wlodawer, A. (1991) *Proc. Natl. Acad. Sci. U.S.A. 88*, 502−506.
Beall, C. J., Mahajan, S., & Kolattukudy, P. E. (1992) *J. Biol. Chem. 267*, 3455−3459.
Ben-Baruch, A., Xu, L., Young, P. R., Bengali, K., Oppenheim, J. J., & Wang, J. M. (1995) *J. Biol. Chem. 270*, 22123−22128.
Brown, K. D., Zurawski, S. M., Mosmann, T. R., & Zurawski, G. (1989) *J. Immunol. 142*, 679−687.
Brünger, A. T. (1992) *X-PLOR Version 3.1 Manual*, Yale University, New Haven, CT.
Burley, S. K., & Petsko, G. A. (1988) *Adv. Protein Chem. 39*, 125−189.
Burrows, S. D., Doyle, M. L., Murphy, K. P., Franklin, S. G., White, J. R., Brooks, I., McNulty, D. E., Scott, M. O., Knutson, J. R., Porter, D., Young, P. R., & Hensley, P. (1994) *Biochemistry 33*, 12741−12745.
Chung, C.-w., Cooke, R. M., Proudfoot, A. E. I., & Wells, T. N. C. (1995) *Biochemistry 34*, 9307−9314.
Clark-Lewis, I., Shumacher, C., Baggiolini, M., & Moser, B. (1991) *J. Biol. Chem. 266*, 23128−23134.
Clore, G. M., & Gronenborn, A. M. (1991) *J. Mol. Biol. 217*, 617−620.
Clore, G. M., & Gronenborn, A. M. (1995) *FASEB J. 9*, 57−62.
Clore, G. M., Appella, E., Yamada, M., Matsushima, K., & Gronenborn, A. M. (1990) *Biochemistry 29*, 1689−1696.
Clubb, R. T., Omichinski, J. G., Clore, G. M., & Gronenbron, A. M. (1994) *FEBS Lett. 338*, 93−97.
Combadiere, C., Ahuja, S. K., Van Damne, J., Tiffany, H. L., Gao, J.-L., & Murphy, P. M. (1995) *J. Biol. Chem. 270*, 29671−29675.
Covell, D. G., Smythers, G. W., Gronenborn, A. M., & Clore, G. M. (1994) *Protein Sci. 3*, 2064−2072.
Dahinden, C. A., Geiser, T., Brunner, T., Von Tscharner, V., Caput, D., Ferrara, P., Minty, A., & Baggiolini, M. (1994) *J. Exp. Med. 179*, 751−756.
Delaglio, F., Grzesiek, S., Vuister, G. W., Zhu, G., Pfeifer, J., & Bax, A. (1995) *J. Biomol. NMR 6*, 277−293.
Eccles, C., Güntert, P., Billeter, M., & Wüthrich, K. (1991) *J. Biomol. NMR 1*, 111−130.
Faitbrother, W. J., Reilly, D., Colby, T. J., Hesselgesser, J., & Horuk, R. (1994) *J. Mol. Biol. 242*, 252−270.
Franci, C., Wong, L. M., Van Damne, J., Proost, P., & Charo, I. F. (1995) *J. Immunol. 154*, 6511−6517.
Gayle, R. B., III, Sleuth, P. R., Birks, C. W., Weerawarna, K. S., Ceretti, D. P., Kozlovsky, C. J., Nelson, N., Vanden Bos, T., & Beckmann, M. P. (1993) *J. Biol. Chem. 268*, 7283−7289.
Griesenger, C., Otting, G., Wüthrich, K., & Ernst, R. R. (1988) *J. Am. Chem. Soc. 110*, 7870−7872.
Güntert, P., Braun, W., Billeter, M., & Wüthrich, K. (1989) *J. Am. Chem. Soc. 111*, 3997−4004.
Güntert, P., Braun, W., & Wütrich, K. (1991a) *J. Mol. Biol. 217*, 517−530.
Güntert, P., Qian, Y. Q., Otting, G., Müller, M., Gehring, W., & Wüthrich, K. (1991b) *J. Mol. Biol. 217*, 531−540.
Güntert, P., Berndt, K. D., & Wüthrich, K. (1993) *J. Biomol. NMR 3*, 601−606.
Havel, T., & Wüthrich, K. (1984) *Bull. Math. Biol. 46*, 673−698.
Havel, T. F. (1991) *Prog. Biophys. Mol. Biol. 56*, 43−78.
Herbert, C. A., Vitangcol, R. V., & Baker, J. B. (1991) *J. Biol. Chem. 266*, 18989−18994.
Hutchinson, E. G., & Thornton, J. M. (1993) *Protein Eng. 6*, 233−245.
Jeener, J., Meier, B. H., Bahmann, P., & Ernst, R. R. (1979) *J. Chem. Phys. 71*, 4546−4553.
Kelner, G. S., & Zlothnik, A. (1995) *J. Leukocyte Biol. 57*, 778−781.
Kelner, G. S., Kennedy, J., Bacon, K. B., Kleyensteuber, S., Largaespada, D. A., Jenkins, N. A., Copeland, N. G., Bazan, J. F., Moore, K. W., Schall, T. J., & Zlotnik, A. (1994) *Science 266*, 1395−1398.
Kennedy, J., Kelner, G. S., Kleyensteuber, S., Schall, T. J., Weiss, M. C., Yssel., H., Schneider, P. V., Cocks, B. G., Bacon, K. B., & Zlothnik, A. (1995) *J. Immunol. 155*, 203−209.
Kim, K.-S., Clark-Lewis, I., & Sykes, B. D. (1994) *J. Biol. Chem. 269*, 32909−32915.
Kim, K.-S., Rajarathnam, K., Clark-Lewis, I., Sykes, B. D. (1996) *FEBS Lett. 395*, 277−282.
Kraulis, P. J. (1991) *J. Appl. Crystallogr. 24*, 946−950.
Kumar, A., Ernst, R. R., & Wütrich, K. (1981) *Biochem. Biophys. Res. Commun. 95*, 1−6.
Lodi, P. J., Garrett, D. S., Kuszewski, J., Tsang, M. L.-S., Weatherbee, J. A., Leonard, W. J., Gronenborn, A. M., & Clore G. M. (1994) *Science 263*, 1762−1767.
Lubkowski *et al.* (1997) *Nat. Struct. Biol. 4*, 64−69.
Malkowski, M. G., Wu, J. Y., Lazar, J. B., Johnson, P. H., & Edwards, B. F. P. (1995) *J. Biol. Chem. 270*, 7077−7087.
Marion, D., & Wütrich, K. (1983) *Biochem. Biophys. Res. Commun. 113*, 967−974.
Minty, A., Chalon, P., Guillemot, J. C., Kaghad, M., Liauzun, P., Magazin, M., Miloux, B., Minty, C., Ramond, P., Vita, N., Lupker, J., Shire, D., Ferrara, P., & Caput, D. (1993) *Eur. Cytokine Network 4*, 99−110.
Moser, B., Dewald, B., Barella, L., Schumacher, C., Baggiolini, M., & Clark-Lewis, I. (1993) *J. Biol. Chem. 268*, 7125−7128.
Noso, N., Proost, P., Van Damne, J., & Schröder, J.-M. (1994) *Biochem. Biophys. Res. Commun. 200*, 1470−1476.
Opdenakker, G., Froyen, G., Fiten, P., Proost, P., & Van Damne, J. (1993) *Biochem. Biophys. Res. Commun. 191*, 535−542.
Oppenheim, J. J., Zachariae, C. O. C., Mukaida, N., & Matsushima, K. (1991) *Annu. Rev. Immunol. 9*, 617−648.
Paolini, U. F., Willard, D., Conster, T., Luther, M., & Krangel, M. S. (1994) *J. Immunol. 153*, 2704−2717.
Piotto, M., Saudek, V., & Sklenar, J. (1992) *J. Biomol. NMR 2*, 661−666.
Proost, P., Wuyts, A., & Van Damne, J. (1996) *J. Leukocyte Biol. 59*, 67−74.
Rajarthnam, K., Skyes, B. D., Kay, C. M., Dewald, B., Geiser, T., Baggiolini, M., & Clark-Lewis, I. (1994) *Science 264*, 90−92.
Richardson, J. S. (1981) *Adv. Protein Chem. 34*, 167−339.
Roussel, A., & Cambillau, C. (1989) in *Silicon Graphics Geometry Partner Directory* (*Fall 1989*) (Silicon Graphics, Ed.) pp 77−78, Silicon Graphics, Moutain View, CA.
Schall, T. J. (1991) *Cytokine 3*, 165−183.
Sherry, B., & Cerami, A. (1991) *Curr. Opin. Immunol. 3*, 56−60.
Sibanda, B. L., & Thornton, J. M. (1985) *Nature 316*, 170−174.
Skelton, N. J., Aspiras, F., Ogez, J., & Schall, T. J. (1995) *Biochemistry 34*, 5329−5342.
Sklenar, V., Piotto, M., Leppik, R., & Saudek, V. (1993) *J. Magn. Reson. A 102*, 241−245.
Sozzani, S., Zhou, D., Locati, M., Rieppi, M., Proost, P., Magazin, M., Vita, N., Van Damne, J., & Mantovani, A. (1994) *J. Immunol. 152*, 3615−3622.
St. Charles, R., Walz, D. A., & Edwards, B. F. P. (1989) *J. Biol. Chem. 264*, 2092−2099.
Szyperski, T., Güntert, G., Otting, G., & Wüthrich, K. (1992) *J. Magn. Reson. 99*, 552−560.
Tanaka, S., Robinson, E. A., Yoshimura, T., Matsushima, K., Leonard, E. J., & Appella, E. (1988) *FEBS Lett. 236*, 467−470.
Tanaka, Y., Adams, D. H., Hubscher, S., Hirano, H., Siebenlist, U., & Shaw, S. (1993) *Nature 361*, 79−82.
Valente, A. J., Rozek, M. M., Schwartz, C. J., Graves, D. T. (1991) *Biochem. Biophys. Res. Commun. 176*, 309−314.
Van Damne, J., Proost, P., Lenearts, J.-P., & Opdenakker, G. (1992) *J. Exp. Med. 176*, 59−65.
Wishart, D. S., Sykes, B. D., & Richards, F. M. (1992) *Biochemistry 31*, 1647−1651.
Wüthrich, K. (1986) *NMR of Proteins and Nucleic Acids*, John Wiley and Sons, New York.
Yoshida, T., Imai, T., Kakizadi, M., Nishimura, M., & Yoshie, O. (1995) *FEBS Lett. 360*, 155−159.
Zhang, X., Chen, L., & Bancroft, D. P. (1994) *Biochemistry 33*, 8361−8366.
Zhang, Y. J., Rutlegde, B. J., & Rollins, B. J. (1994) *J. Biol. Chem. 269*, 15918−15924.

BI9627929